



# Photocatalytic rate dependence on light absorption properties of different TiO<sub>2</sub> specimens

Paola Calza, Marco Minella, Luca Demarchis, Fabrizio Sordello, Claudio Minero\*

Università di Torino, Dipartimento di Chimica and Nanostructured Interfaces and Surfaces Inter-departmental centre, Via Giuria 5, 10125 Torino, Italy

## ARTICLE INFO

The authors dedicate this work to the memory of professor E. Pelizzetti (16 February 1944–25 July 2017) – University of Torino, Italy – for his pioneering research in heterogeneous photocatalysis, which inspired many of the papers cited in this work.

### Keywords:

Photocatalysis  
TiO<sub>2</sub> specimens  
Kinetic analysis  
Scattering  
Absorption coefficient  
Formic acid

## ABSTRACT

The light absorption and scattering play a prominent and often underrated role in the overall photocatalytic process and heavily affect the rate. This is particularly important for the choice of the catalyst in addition to other chemical and physical parameters usually considered for their catalytic role. Here we propose an approximated but easy-to-apply method to evaluate the light harvested by the photocatalyst slurry and its scattering/absorption coefficients, which does not require the use of complex spectrophotometric tools and the complicated radiative transport equation. The optical properties are obtained with the lamp and in the experimental setup employed in the photocatalytic batch tests. Among the four TiO<sub>2</sub> specimens considered, we characterized Evonik P25 and Hombikat UV100. The obtained scattering and absorption coefficients helped in rationalizing the experimental results on the degradation of formic acid at low concentration. From the rate dependence on the catalyst concentration, this approach allowed further understanding of the role of catalyst-specific properties affecting the overall catalytic performance. This approach is proposed as a starting point for fixing conditions to compare different photocatalysts.

## 1. Introduction

In the last decades many reports demonstrated that heterogeneous photocatalysis has unrivalled ability to abate persistent pollutants often until complete mineralization [1–5]. Nevertheless, commercial applications are still limited, because of the low efficiency in terms of low quantum yield and of the scarce ability of the most active photocatalysts to absorb solar light, increasing the costs and the requirements for water-treatment plants [6].

The fundamentals of semiconductor photocatalysis are now well understood, and there is a general consensus that the photocatalytic process starts with the absorption of a photon (with energy  $h\nu$ ) from a semiconductor characterized by an energy gap  $E_g$  lower than the photon energy ( $h\nu \geq E_g$ ). This photoexcitation causes a change of the redox properties of the semiconductor surface, allowing charge transfer reactions through the semiconductor/solution interface [7]. The net result is the oxidation of the dissolved contaminants and the reduction of the electron acceptor – usually molecular oxygen and/or a reducible adsorbed substrate [8] – catalyzed by the irradiated semiconductor [9,10]. Besides this apparent simplicity, the overall photocatalytic rate is the result of the complex interplay among many elementary reactions, whose relative importance is a complicated, and usually not reported function of the experimental setup and type of catalyst. An

exhaustive mathematical treatment of the photocatalytic process results very complex and is still object of debate.

Several treatments to describe the photocatalytic rate have been proposed. One of the first and most successful models was the Langmuir-Hinshelwood (L-H) [7,11,12], which describes the degradative process in conditions of substrate adsorption at the catalysts surface. *Per se* the L-H treatment would be correct if the surface concentrations of reactive species, namely free or trapped electrons and holes, were fixed and constant, which is usually not the case. In general, these concentrations are function of the incident photon flux and the substrate nature and concentration. Conversely, the adsorption constants derived from the L-H model decrease with increasing light intensity, while the rate constant increases [13]. Therefore, L-H kinetic model cannot describe the overall rate, as demonstrated by Emeline and co-workers [14] and by Minero and Vione [15]. Despite the large agreement on the inadequacy of L-H model to interpret photocatalytic kinetic data [7], it is largely diffuse the habit to correlate uncritically the Langmuir adsorption coefficients of the studied substrate with the related kinetic data forgetting that: *i*) the literature demonstrated the inadequacy of this model [16]; *ii*) the best isotherm describing the adsorption of a molecules on the surface of the most diffused photocatalysts is the Freundlich isotherm [17] and not the Langmuir one, although the last is useful for simple modelling. In 2007, Salvador and

\* Corresponding author.

E-mail address: [claudio.minero@unito.it](mailto:claudio.minero@unito.it) (C. Minero).

<https://doi.org/10.1016/j.cattod.2018.10.013>

Received 31 July 2018; Received in revised form 5 October 2018; Accepted 8 October 2018

Available online 23 October 2018

0920-5861/ © 2018 Elsevier B.V. All rights reserved.

co-workers [18] – based on the model of reference [15] – developed the “Direct-Indirect” (D-I) kinetic model, assuming two different kinds of charge transfer to solution species, namely adiabatic and inelastic. The model was able to fit different sets of experimental data better than the L-H model [19], but still unsatisfactory, as in 2011 Rios et al. [20] stressed again the importance of back-reactions in the photocatalytic process, previously and largely supported by Minero and co-workers [11,19,21].

All these models highlight the importance of the chemical phenomena involved in the photocatalytic process, like adsorption, back-reactions, charge transfer dynamic and recombination. However, the light harvesting plays an equally important role in determining the rate, [15] as highlighted in the recent review by Egerton [22]. The optical properties of the semiconductor slurry are strongly related even with the state of agglomeration of the primary particles that dramatically influences the overall extinction properties (scattering and absorption) and ultimately the kinetics of the photocatalytic process [22,23]. As a consequence, the particle dispersion determines the photocatalytic activity, owing to changes in slurry optical features and, therefore, suitable control experiments should be designed [22]. The importance of light absorption by the photocatalyst in the overall photocatalytic process has been evidenced by the impressive research efforts spent in the 3D structuration of photocatalysts to improve their performance [24]. The fact that semiconductor photonic crystals performed better compared with their nanoparticle homologues witnesses that light absorption and efficient light use by the photocatalyst allow significant room for the improvement of the performance [25,26].

This work focuses on the effects of optical properties of some titanium dioxide specimens and on the evaluation of their role on the photocatalytic efficiency. We propose a simple experimental approach to estimate the optical parameters of slurries in the same apparatus that can be used to carry out the photocatalytic experiments. This procedure was applied to two different commercial TiO<sub>2</sub> specimens (Evonik P25 and Hombikat UV100). Furthermore, the relationship between the optical parameters and the kinetics of the photocatalytic process was assessed by monitoring formic acid transformation in the presence of the same TiO<sub>2</sub> photocatalysts at different loadings.

## 2. Theoretical background

Among many possible kinetic models, the quadratic kinetic model [15] gives a rate expression that is able to correctly predict the dependence on incident light intensity, initial substrate concentration and catalyst loading. This model was extensively validated [27], and has the advantage of having only one kinetic parameter, thus only one degree of freedom, that can help to avoid overfitting [28]. To determine and measure the influence played by the optical parameters of titanium dioxide suspensions on their photocatalytic efficiency we started from the expression of quantum yield  $\eta$  in the case of a photocatalytic process characterized by current doubling (see paragraph 4.2) [15]:

$$\eta = -\frac{y}{2} + \sqrt{\frac{y}{2}\left(\frac{y}{2} + 2\right)} \quad (1)$$

where the dimensionless master variable  $y = k_0 C_{Red1} C_{Ox2} \phi_v^{-1}$ , in which  $k_0$  is a cumulative kinetic constant (*vide infra*),  $C_{Red1}$  and  $C_{Ox2}$  are the molar concentrations of the substrate and the oxidant in the system as a whole (semiconductor surface + water bulk, mol L<sup>-1</sup>) and  $\phi_v$  is the volumetric rate of radiation absorption (mol L<sup>-1</sup> s<sup>-1</sup>). Eq. (1) is a simplification of a more general one, in which a second dimensionless variable  $\zeta$ , expressing the net fraction of light-generated charge carriers that reach the surface, was present. In the model here adopted  $\zeta = 1$ . In the case of larger particles where resistance to charge carriers transfer to the surface could be present, or when absorbed light is large,  $0 < \zeta < 1$ . This would change only the relative scalar value of effective light absorbed.

In the limit of low quantum yield,  $\frac{y}{2} \ll 2$ , Eq. (1) can be approximated to:

$$\eta = -\frac{y}{2} + \sqrt{y} \quad (2)$$

This relationship holds true when: *i*)  $k_0$  is small, i.e. the photocatalytic process is hindered because of large recombination and/or sluggish charge transfer at the surface; *ii*)  $C_{Red1}$  and/or  $C_{Ox2}$  are small, thus favouring recombination over charge transfer; *iii*)  $\phi_v$  is large compared with  $k_0 C_{Red1} C_{Ox2}$ , which means that the recombination processes (*second* order with respect to the charge carrier concentrations) overcome the charge transfer kinetics (*first* order with respect to the charge carrier concentrations).

The rate of the photocatalytic process is given by definition as the product of quantum yield and volumetric rate of absorption. Then

$$\frac{rate}{C_{cat}} = -\frac{k'}{2} + \sqrt{\frac{k' \phi_v}{C_{cat}}} \quad (3)$$

in which  $k' C_{cat} = k_0 C_{Red1} C_{Ox2}$ . In a one-dimensional photocatalytic reactor, like that used in batch experiments where a container is illuminated from the top, the light intensity is a function of the optical depth  $z$ , and, consequently, the volumetric rate of absorption  $\phi_v(z)$  can be expressed as  $\phi_v(z) = \kappa(\lambda) I(z) 10^3$ , where  $\kappa(\lambda)$  represents the wavelength dependent absorption coefficient (cm<sup>-1</sup>) and  $I(z)$  is the radiation intensity at the depth  $z$  inside the solution in mol s<sup>-1</sup> cm<sup>-2</sup>. The observed rate is the integral of Eq. (3) over the overall optical depth  $b$ :

$$\frac{rate_{obs}}{C_{cat}} = -\frac{k'}{2} + \frac{1}{b} \int_0^b \sqrt{\frac{k' \phi_v(z)}{C_{cat}}} dz \quad (4)$$

Introducing the expression of  $\phi_v(z)$  in Eq. (4), and considering  $\kappa(\lambda) = 10^{-3} \ln(10) \epsilon_{abs}(\lambda) C_{cat}$  (where  $\epsilon_{abs}$  is the specific absorption coefficient in cm<sup>2</sup> g<sup>-1</sup>), one obtains Eq. (5):

$$\frac{rate_{obs}}{C_{cat}} = -\frac{k'}{2} + \sqrt{\ln(10) I_0 k' \epsilon_{abs}(\lambda) \chi} \quad (5)$$

in which  $I_0$  is the incident radiation intensity at the top of the slurry expressed in mol s<sup>-1</sup> cm<sup>-2</sup> and  $\chi$  is the dimensionless average square root of normalized absorbed light in the reactor expressed as:

$$\chi = \frac{1}{b} \int_0^b \sqrt{\frac{I(z)}{I_0}} dz \quad (6)$$

It is often not recognized that the rate expressed in Eq. (5) provides a saturative dependence on the substrate concentration. Almost the same behaviour is provided by the L-H equation, but from an erroneous starting-point [16]. The kinetic relationship (5) has general applicability, independently on the optical and morphological properties of particles, provided that the slurry is sufficiently stable regarding sedimentation. The application of Eq. (5) needs that the hypotheses under which it was derived are fulfilled, namely that: 1)  $y \ll 4$  (that is low quantum yield regime). For quantum yield  $< 0.3$ – $0.4$  the approximated equation is always valid. In the case that  $\zeta$  (see above) were  $< 1$ , this would proportionally reduce the maximum quantum yield for which the model is applicable; 2) the original model does not take into account the back reactions, which could be present with some substrates. This is not the case for formic acid here used as substrate.

The intensity of the light as a function of the optical depth can be approximated with the Kubelka–Munk (K-M) equation: [15]

$$I(z) = \frac{v I_0}{u \sinh(v\sigma z) + v \cosh(v\sigma z)}; \text{ with } u = 1 + \frac{\kappa(\lambda)}{\sigma(\lambda)}, \text{ and with } v = \sqrt{u^2 - 1} \quad (7)$$

where the parameters  $\sigma(\lambda)$  and  $\kappa(\lambda)$  represent the wavelength dependent scattering and absorption coefficients in cm<sup>-1</sup>. Eq. (7) reduces to the Lambert–Beer law for  $\sigma \rightarrow 0$ :

$$I(z) = I_0 e^{-\kappa z} \quad (8)$$

The K-M equation explicitly gives the transmittance as a function of the optical path  $z$  using scattering and absorption optical constants. It will be used to obtain these parameters from experimental transmittance. Rigorously, Eq. (7) could only be applied when monochromatic light is employed, or when the emission spectral range is sufficiently narrow that the variations of the optical constants are negligible compared with the uncertainty of the adopted technique. The approximation involved in K-M equation and its accuracy was studied using the numerical solution of the integro-differential radiative transfer equation (RTE) for the sparse distribution of spherical scatterers. Except for low optical thickness, the relative errors are under few percent [29]. The numerical solution of RTE was used in reactor modelling and for the evaluation of absorbed light [30,31]. The use of a more complex tool like the numerical solution of RTE to fit experimental data is obviously possible although requiring skills not available in all laboratories. The comparison with optical parameters obtained using K-M and the reported values obtained through the RTE solution is discussed later.

Here the integration along the irradiated slurry depth according to Eq. (6) was performed numerically on experimental data. An explanatory scheme of the adopted procedure to evaluate the optical properties of the investigated photocatalyst is reported in Fig. 1-SM of the Supplementary Material, hereafter SM.

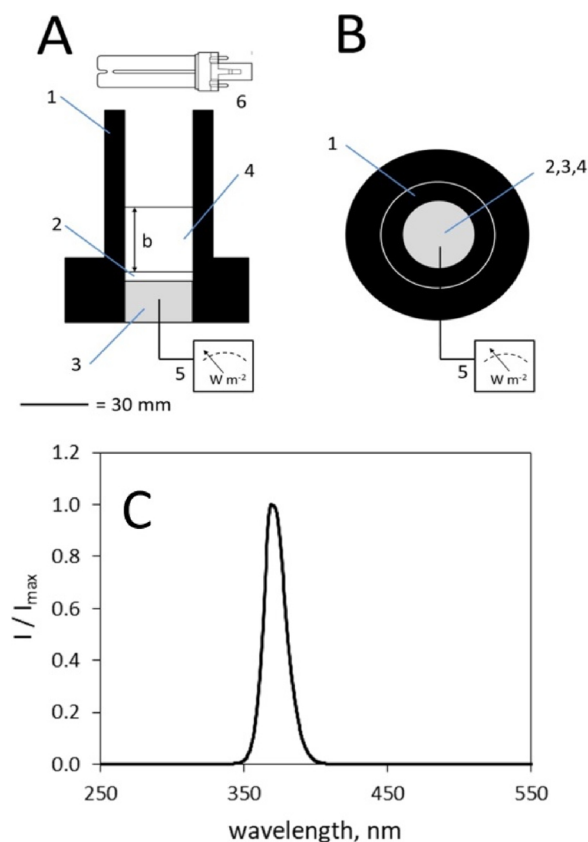


**Fig. 1.** System used for the determination of the optical properties of  $\text{TiO}_2$  suspensions. (A) Transversal section; (B) view from above and (C) emission spectrum of the Philips PL-S 9W BLB lamp normalized for the emission maximum. 1) HDPE walls; 2) optical glass disk; 3) UV probe; 4)  $\text{TiO}_2$  suspension with depth  $b$ ; 5) irradiance meter; 6) UV source.

### 3. Experimental

#### 3.1. Reagents and materials

Formic acid (99%) was purchased from Riedel-de Haën, hydrochloric acid (37%) from Carlo Erba, potassium hydroxide (> 99%) from Sigma-Aldrich. In this work four different types of commercial titanium dioxide were used: Evonik P25 (BET area ca  $50 \text{ m}^2 \text{ g}^{-1}$ , 80% anatase/20% rutile), Hombikat UV100 (BET area ca  $348 \text{ m}^2 \text{ g}^{-1}$ , 100% anatase), Merck  $\text{TiO}_2$  (BET area ca  $10 \text{ m}^2 \text{ g}^{-1}$ , 100% anatase) and Wackherr  $\text{TiO}_2$  (BET area ca  $8.5 \text{ m}^2 \text{ g}^{-1}$ , 100% anatase). The water used in all the experiments was of Milli-Q® quality. Titanium dioxide water suspensions were prepared by sonication with a 205 W Branson 2200 sonicator for 15 min.

#### 3.2. Determination of optical properties

The optical properties of each titanium dioxide specimen were determined through the evaluation of the  $\chi$  parameter through the measure of the transmittance as a function of the concentration of the semiconductor suspensions, recording the intensity of the light transmitted as a function of the optical path  $b$ .

For an accurate measurement of the transmission and of the  $\chi$  parameter, a custom-built cylindrical cell in black HDPE was used. This cell was fitted with an optical glass disk in the bottom (transmittance at  $365 \text{ nm} \approx 100\%$ , width = 5 mm), which allows the transmission of light and acts as support for  $\text{TiO}_2$  suspensions. The UV probe with cosine correction working in the range 290–400 nm was housed immediately below the glass disk. The transmitted light was recorded using a CO.FO.ME.GRA (Milan, Italy) Solarbox Multimeter connected with the probe. A schematic representation of the device is reported in Fig. 1A, B. Data for the evaluation of the  $\chi$  parameter were obtained in a very short timescale (i.e. less than a minute), by measuring the transmission of few aliquots with fixed volume at a given  $C_{\text{cat}}$ . The numerous transmittance measures for optical parameter evaluation required longer time to be carried out (in the order of tens of minutes). These measurements at different optical depths  $b$  were carried out adding stepwise 0.5 mL of suspensions with diverse concentrations of  $\text{TiO}_2$ . In this temporal range the only titania specimens with sufficient stability were Evonik P25 and Hombikat UV100. The value of  $b$  was calculated from the known diameter of the cell. The maximum  $b$  was limited to 12 mm, a value much lower than the height of the cell (70 mm from the top of glass), to avoid cosine error from the illuminating source. The UV source was a 9 W Philips PL-S lamp with an emission maximum at 360 nm (the normalized emission spectrum of the lamp is reported in Fig. 1C). It was positioned horizontally with respect to the cell as evidenced on Fig. 1A (not in scale).

#### 3.3. Irradiation experiments

Samples containing  $\text{TiO}_2$  0.1–1.0  $\text{g L}^{-1}$  and formic acid 0.2–1.0 mM were put into cylindrical Pyrex glass cells (4.0 cm diameter, 2.5 cm height). The UV source was the same used for the measurement of the optical properties. To ensure a controlled illumination distribution in the system, Pyrex cells were put into a home-made black HDPE container with the same size and geometry of the one described above for the optical measurements. Experiments were carried out in the presence of magnetic stirring. Samples were held for several hours in the dark to reach the absorption equilibrium of formic acid on the catalyst surface before the start of the irradiation. The photon irradiance at the top of the cells was  $20.3 \text{ W m}^{-2}$  in the 290–400 nm range, corresponding to  $6.1 \times 10^{-9} \text{ mol s}^{-1} \text{ cm}^{-2}$  considering 365 nm as the average wavelength of the photons emitted by the lamp.

After irradiation, samples were brought to pH 2 with hydrochloric acid to protonate formic acid and remove adsorbed molecules from the catalyst surface. After acidification, suspensions were filtered through

0.45  $\mu\text{m}$  membranes (PTFE, Millipore), the pH was re-established with potassium hydroxide, and then analysed. The profiles of photocatalytic degradation of HCOOH were well described with first order kinetic equation  $[F]_t = [F]_0 \exp(-k_{\text{obs}}t)$  where  $[F]_t$  is the formic acid concentration at time  $t$ ,  $[F]_0$  the initial concentration and  $k_{\text{obs}}$  the observed pseudo-first-order degradation rate constant. The initial degradation rate of formic acid was calculated as  $k_{\text{obs}}[F]_0$ .

### 3.4. Analytical determinations

The analysis of formate was carried out by means of ion chromatography with a Dionex DX 500 instrument equipped with an ED40 conductivity detector, a LC30 chromatography oven, a GP40 pump, an AS9-HC ion exchange column (250 mm x 4 mm i.d.), an ION PAC AG9-HC pre-column and an ASRS-ULTRA 4 mm suppressor. Formic acid was eluted with 80/20 mixture of  $\text{K}_2\text{CO}_3$  9 mM/Milli-Q water with a flow rate of  $0.9 \text{ mL min}^{-1}$  and with an SRS current of 100 mA. Under these conditions, the retention time for formic acid was 4.95 min.

## 4. Results and discussion

### 4.1. Optical properties of $\text{TiO}_2$ suspensions

Fig. 2 shows the value of  $\chi$  for the four different commercial  $\text{TiO}_2$  investigated as a function of the concentration of the photocatalyst. The  $\chi$  values were obtained by integrating the transmitted light intensity as a function of the optical path  $b$ , according with the definition of the parameter  $\chi$  in the Eq. (6), up to a maximum  $b_{\text{max}} = 12 \text{ mm}$ .

The parameter  $\chi$  decreases with the increment of  $C_{\text{cat}}$  for each catalyst. This is in agreement with the definition of  $\chi$ , as an increase in the semiconductors concentration leads to an enhanced intensity of light scattering and absorption, decreasing the average rate of absorption when considering the whole reactor. As the rate normalized for  $C_{\text{cat}}$  depends linearly on  $\chi$  (Eq. (5)), catalysts with more negative slope in Fig. 2 are more subject to the so called *shielding effect* which is often invoked to explain the bell-shaped profile of the photocatalytic rate of a process as a function of the catalyst loading of the slurry [15,32], also for organic photocatalysts [33]. With larger negative slopes, at the same  $C_{\text{cat}}$ , the strong extinction (scattering + absorption) in the very first layers of the irradiated slurry hinders photons to reach the bottom of the reactor decreasing the observed rate, which is averaged on the whole volume of the reactor.

$\text{TiO}_2$  Evonik P25 is characterized by the lowest values of  $\chi$ . This happens because P25 is characterized by a high intensity of scattering of the incident light compared with the other  $\text{TiO}_2$  specimens (see also later for a discussion) [34].

According to the Eq. (5), a catalyst at a given  $C_{\text{cat}}$  with a high  $\chi$  could provide a degradation rate higher than that for a semiconductor

with lower  $\chi$  values. This relationship is useful to compare the photocatalytic efficiency among different kinds of materials, and might allow the development of new types of catalysts with high efficiency by monitoring their optical properties.

The dependence of transmitted light intensity both on  $b$  value and catalyst concentration was carefully studied on Evonik P25 suspensions with loadings from  $0.05$  to  $0.6 \text{ g L}^{-1}$ , and from  $0.05$  to  $1.0 \text{ g L}^{-1}$  for Hombikat UV100. The different loading ranges were chosen because the larger extinction of P25 suspensions hinders the accurate determination of the light transmitted for larger loadings, even for short optical depths. The raw data are reported in Fig. 2-SM. Each observed dependence on  $b$  values at fixed  $C_{\text{cat}}$  is well described by the Lambert-Beer law (where attenuation is due to the extinction coefficient) or alternatively by Eq. (7) (see later), with the exception of the data at very low optical depth, especially with larger catalyst loadings. In these conditions the measured extinction is lower than the predicted one, as a consequence of possible interfering optical phenomena, like the formation of a convex meniscus acting as a lens, which converges the light onto the centre of the probe body. This effect should be more important at low  $b$  and at large  $C_{\text{cat}}$  and could not be completely compensated by the adopted cosine corrector.

For each catalyst the entire dataset (dependence on  $b$  and  $C_{\text{cat}}$ ) was fitted with Eq. (7) to obtain specific coefficients for absorption ( $\epsilon_{\text{abs}}$ ) and scattering ( $\epsilon_{\text{sca}}$ ), which are related to the Kubelka-Munk coefficients  $\kappa$  and  $\sigma$  according to the following equations:

$$\epsilon_{\text{abs}}(\lambda) = \frac{\kappa(\lambda) 10^3}{\ln(10)C_{\text{cat}}} \quad (9a)$$

$$\epsilon_{\text{sca}}(\lambda) = \frac{\sigma(\lambda) 10^3}{\ln(10)C_{\text{cat}}} \quad (9b)$$

Fig. 3A,B show the experimental data used to carry out the fit together with the fit curves. They described quite well the experimental data. For each catalyst all the data were fit with  $\epsilon_{\text{abs}}$  and  $\epsilon_{\text{sca}}$  as the only fit parameters, considering for each profile the actual catalyst loading. Surprisingly, although the simplest approximation for absorption/scattering, the K-M equation works quite well, as reported for a variety of other experimental situations [35].

The lamp emission spectrum is narrow and the spectral variations of the optical constants could be considered minor. In the case of polychromatic light the approach here proposed can still be employed, but the obtained optical constants would have an empirical and average meaning only. They allow comparing the properties of different photocatalysts under real illumination conditions, but can only be partially compared with the values measured with monochromatic light.

The fit parameters are reported in Table 1 together with the ratio between  $\epsilon_{\text{sca}}$  and  $\epsilon_{\text{abs}}$ . The specific absorption coefficient for  $\text{TiO}_2$  P25 is five times larger than that of  $\text{TiO}_2$  UV100, while the specific scattering coefficient is roughly 2 times larger for  $\text{TiO}_2$  P25, as also observed in ref. [34]. The ratio between the coefficients is 4 and 9 for P25 and UV100, respectively, suggesting that – from an optical point of view – P25 better exploits the incident light than UV 100, despite of the higher  $\epsilon_{\text{sca}}$ . The larger absorption coefficient potentially leads to a larger photocatalytic rate. Conversely, the larger scattering coefficient of P25 compared to UV100 limits  $\chi$ , which is always lower for P25 than for Hombikat UV100. The fraction of light scattered does not contribute to the overall rate and ultimately represents an unused contribution.

The data of Table 1, including the  $\epsilon_{\text{sca}}$  to  $\epsilon_{\text{abs}}$  ratios, are of the same order of magnitude, but significantly lower than those previously reported [34], and in particular of figures 6,7 of ref. [36]. The reason can be easily related to the different adopted procedures and setup. While in ref [34] the incident light is monochromatic, and therefore the optical parameters are referred to a specific wavelength, in this work the parameters obtained are mediated over the range of wavelengths emitted by the used lamp, and effectively used in the cell volume. As it occurs experimentally, because photons scattered outside the lateral

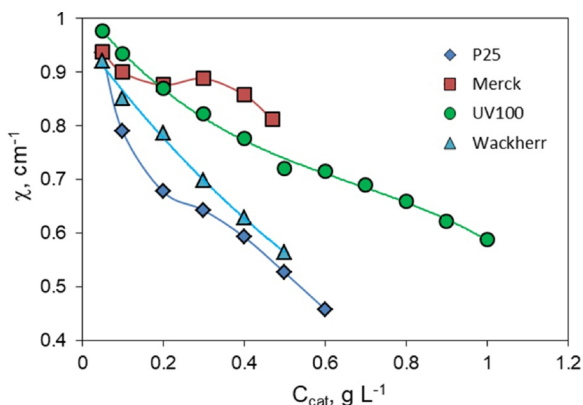
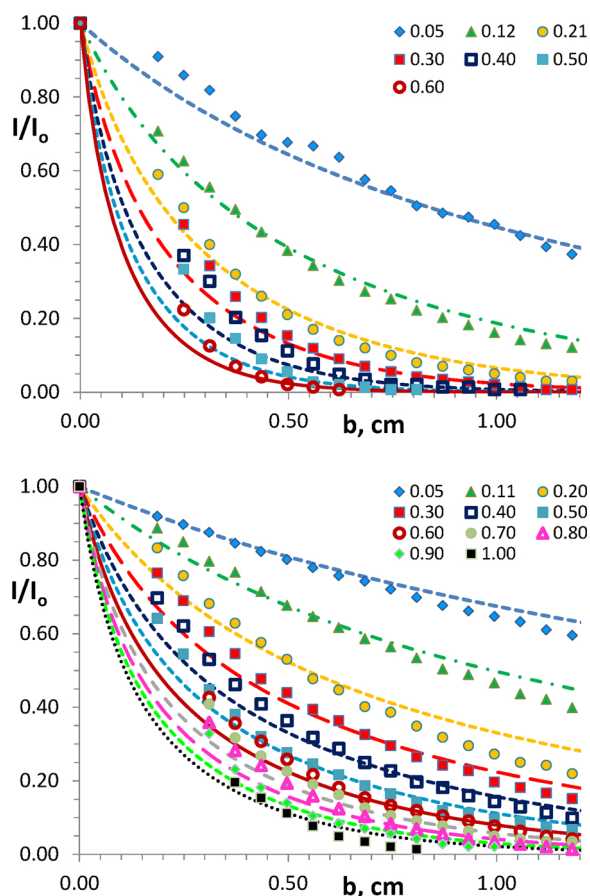


Fig. 2. Values of the parameter  $\chi$  computed through Eq. (6) for different specimens of commercial  $\text{TiO}_2$  at different catalyst concentrations.



**Fig. 3.** Normalized radiation intensity  $I/I_0$  as a function of the optical depth  $b$  and catalyst loading (in  $\text{g L}^{-1}$ , see legend) for Evonik P25 (top) and Hombikat UV100 (bottom) suspensions. For each catalyst the curves were obtained from the best fit of the overall dataset with Eq. (7) with  $\epsilon_{abs}$  and  $\epsilon_{sca}$  as the only fit parameters for the whole set of catalyst loadings.

**Table 1**

Coefficients for scattering  $\epsilon_{sca}$  and absorption  $\epsilon_{abs}$ , and their ratio for  $\text{TiO}_2$  specimens Evonik P25 and Hombikat UV 100.

	Evonik P25	Hombikat UV100
$\epsilon_{sca}, \text{cm}^2 \text{g}^{-1}$	$(6.5 \pm 1.1) \cdot 10^3$	$(3.1 \pm 0.3) \cdot 10^3$
$\epsilon_{abs}, \text{cm}^2 \text{g}^{-1}$	$(1.6 \pm 0.2) \cdot 10^3$	$(0.34 \pm 0.03) \cdot 10^3$
$\epsilon_{sca}/\epsilon_{abs}$ ratio	$4.1 \pm 0.9$	$9.0 \pm 1.7$

walls do not contribute to the photocatalytic process, in the setup here used they are not collected by the detector. Then the obtained values refer only to the lamp used, but are relevant for the (commonly) used

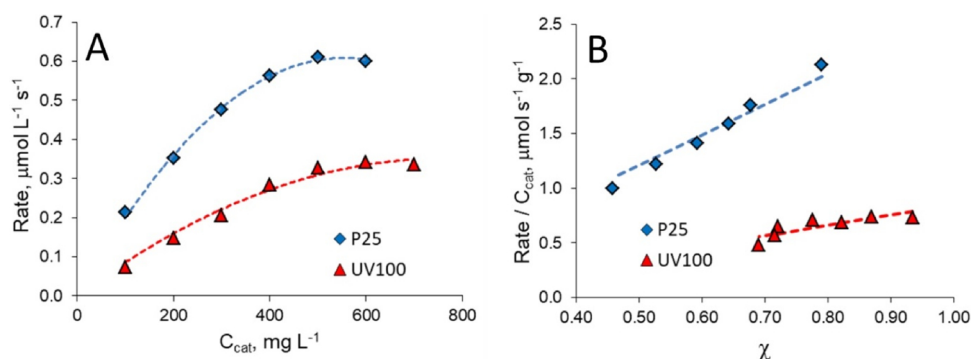


**Fig. 4.** A) HCOOH degradation rates vs.  $C_{cat}$  and B) degradation rates normalized for  $C_{cat}$  as a function of  $\chi$  for  $\text{TiO}_2$  P25 and UV100 at 0.2 mM initial [HCOOH].

experimental setup. In addition, the method here proposed is easier to apply, because it does not require i) the use of a spectrophotometer equipped with total diffuse reflectance accessory as used by Cabrera et al. to evaluate absorption and forward scattering; ii) the application of the quite complex radiative transport equation to obtain the scattering and absorption coefficients [34]. The data reported in Table 1 are more similar to the experimental extinction coefficients reported by Egerton [22], obtained on rutile powders with different particle size. In agreement with Egerton's data, for the photocatalysts here investigated we found a marked decrease in the extinction coefficient with decreasing particle size.

#### 4.2. Photodegradation experiments

The influence of the optical parameters on the degradation rate was evaluated by carrying out formic acid photodegradation experiments in the presence of P25 and UV100 specimens, for which the absorption and scattering coefficients were evaluated. Formic acid was chosen as substrate because it is not subjected to back-reactions [37]. Furthermore, thanks to the extremely reducing potential of the couple  $\text{CO}_2^-/\text{CO}_2$  [38] the formate radical is able to inject an electron into the conduction band evolving directly to  $\text{CO}_2$ . This process is usually reported as current doubling [39–42]. Firstly, we followed the degradation of 0.2 mM formic acid at different concentrations of  $\text{TiO}_2$  suspensions, thus working at significant different  $\chi$  values. This concentration (0.2 mM) was the lowest concentration for which it was experimentally possible to follow the decay profile. At the same time this concentration was supposed to be low enough to allow the approximation  $y/2 \ll 2$ , and, therefore, the use of Eq. (5) to describe the kinetic data.

The time evolution of formic acid for P25 and UV100 at different  $C_{cat}$  are reported in Fig. 3-SM. Fig. 4A shows the rate as a function of  $C_{cat}$ . The rates normalized for the catalyst concentration are reported in Fig. 4B as functions of  $\chi$ . The term  $\text{rate}_{obs}/C_{cat}$  proportionally increases with increasing  $\chi$ , as predicted by Eq. (5), for both catalysts.

The role of factors other than the light scavenging for the two semiconductors was estimated by evaluation of  $k'$  in Eq. (5) through the fit of the data reported in Fig. 4B. In Eq. (5)  $k'$  is the only fit parameter, being known the other terms under the square root, namely  $I_0$  and  $\epsilon_{abs}$ . The nonlinear fit (as  $k'$  is both in the intercept and slope of the straight line) gives the cumulative constant  $k'$ , which is reported with its contributions in Eq. (10): [15]

$$k' = k_{ox,s} k_{red,s} K_{Red1} K_{Ox2} C_{Red1} [Ox_{2,f}] S (2k_{R,s} a_s^2)^{-1} (1 + K_{Ox2} [Ox_{2,f}])^{-1} \quad (10)$$

where  $k_{ox,s}$  and  $k_{red,s}$  are the rate constants for the oxidation and the reduction processes,  $K_{Red1}$  and  $K_{Ox2}$  are the adsorption constants for substrate and the oxidant (in this case oxygen) respectively,  $C_{Red1}$  is the molar concentration of the substrate in solution,  $[Ox_{2,f}]$  is the molar concentration of oxygen in the water bulk,  $S$  is the photocatalyst

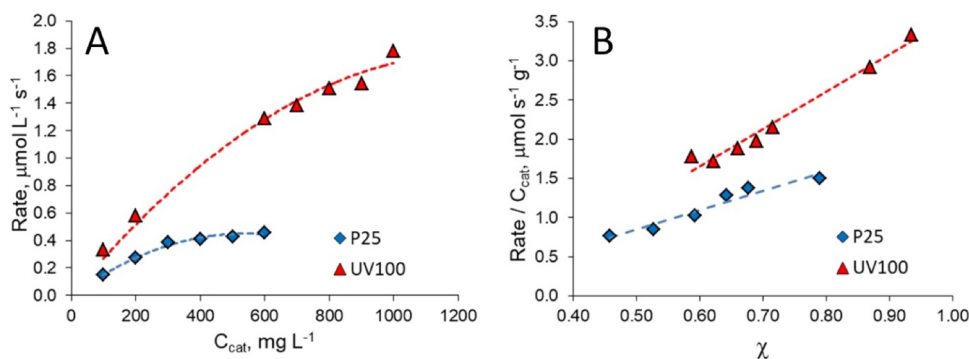


Fig. 5. A) HCOOH degradation rates vs.  $C_{\text{cat}}$  and B) degradation rates normalized for  $C_{\text{cat}}$  as a function of  $\chi$  for  $\text{TiO}_2$  P25 and UV100 at 1.0 mM initial [HCOOH].

specific surface area,  $k_{R,s}$  is the recombination rate constant between surface-trapped electrons and holes,  $a_s$  is the specific area of the exchange site on the photocatalyst surface. The intrinsic (crystallographic phase, surface defects, band potentials, doping, ...) and extrinsic properties (pH, composition of the solution, presence complexing ions, ...) all influence the kinetic and thermodynamic constants included in the parameter  $k'$ .

The obtained values for  $k'$  are 0.36 and 0.22  $\mu\text{mol s}^{-1} \text{g}^{-1}$  for Evonik P25 and for Hombikat UV100, respectively. Dividing  $k'$  by  $C_{\text{RedI}}$  and  $S$  one gets the value of the kinetic cumulative constants independent on the substrate concentration and equal  $k'' = 3.6 \times 10^{-8}$  and  $1.1 \times 10^{-8} \text{ m s}^{-1}$  for Evonik P25 and UV100, respectively. Then the bundle of constants (kinetic and thermodynamic) is about 3 times lower for UV100. The intrinsic heterogeneity of the  $\text{TiO}_2$  P25 structure (with the contemporary presence of two crystallographic phase, anatase and rutile, closely interacting) has been often reported as the driving force able to increase the kinetics of separation of the photo-formed charge carriers and consequently decrease the recombination kinetics [43,44]. Eq. (10) shows that  $k''$  is inversely proportional to the recombination rate constant. Therefore, supposing similar reaction and partitioning constants for P25 and UV100, the lower  $k''$  values for UV100 could be ascribed to a recombination process more marked (larger  $k_{R,s}$ ) on this photocatalyst than on  $\text{TiO}_2$  P25.

A larger concentration of formic acid (1.0 mM) was also tested at different concentrations of  $\text{TiO}_2$  (i.e. at different  $\chi$  values) as done for the lower concentration. The time evolution of formic acid for P25 and UV100 at different  $C_{\text{cat}}$  are reported in Fig. 4-SM. At 1 mM of formic acid it can be observed from Fig. 5A that: i) UV100 outperformed P25, contrarily to the degradations carried out at low concentration; ii) the degradation rate with UV100 was significantly higher than at 0.2 mM; and iii) P25 displayed nearly the same degradation rate at the two formic acid concentrations. Although the rate normalized for  $C_{\text{cat}}$  is linear versus  $\chi$  (Fig. 5B), the fit with Eq. (5) is inconsistent, because the slope, especially for UV100, implies  $\epsilon_{\text{abs}}$  values significantly different from those reported in Table 1. Then at higher concentration the approximation on which Eq. (5) was derived is no more valid, that is  $y/2\alpha^2$  is no more legitimate. It is here useful to recall that  $y$  increases with  $C_{\text{red}}$ . Furthermore, at larger substrate concentration other kinds of surface sites not involved at low concentration could be interested, making the kinetic description of the process more complex, as previously observed for the photocatalytic transformation of glycerol on  $\text{TiO}_2$  P25. [19,21] There it was observed that passing from low to higher concentrations of substrate, there is a change of the basic mechanism of electron transfer, from the direct one (at the interface), favoured by surface complexation, to an indirect one (across the interface), in which the substrate is not bound [37].

## 5. Conclusions

The rate is influenced by a large variety of parameters that are

difficult to evaluate. Under defined conditions we proved that optical properties of catalysts can be easily evaluated, and that their contribution to the overall efficiency can be assessed through the  $\chi$  parameter. The method here proposed can be used to calculate the scattering and absorption properties averaged over the emission spectrum of the lamp employed in the photocatalytic reactor. Consequently, it is possible to easily uncover the most promising photocatalyst from an optical point of view.

The degradation rate of formic acid changes accordingly with the Eq. (5). Experimental data can be properly described by the quadratic kinetic model in the conditions of relatively low quantum yield [15]. Moreover, given the optical parameters, the evaluation of  $k'$  from the  $\text{rate}/C_{\text{cat}}$  vs  $\chi$  plot allows assessing a lumped parameter specific of each catalyst, which includes the base physical processes of charge carriers, catalyst surface area and substrate adsorption constant. This evaluation is not possible when comparing only the rate, mainly if this is obtained at a given  $C_{\text{cat}}$  in a custom experimental setup. The proposed approach can be the starting point for fixing conditions to compare different photocatalysts. In particular, besides the substrate concentration, the catalysts have to be compared to the same  $\chi$  value. This is important in the growing field of the development of new and more efficient photocatalysts.

## Acknowledgements

The financial support from project Ricerca Locale – University of Torino – is gratefully acknowledged.

## References

- [1] A.R. Ribeiro, O.C. Nunes, M.F.R. Pereira, A.M.T. Silva, *Environ. Int.* 75 (2015) 33–51.
- [2] A. Di Paola, E. García-López, G. Marci, L. Palmisano, *J. Hazard. Mater.* 211–212 (2012) 3–29.
- [3] P. Pichat (Ed.), *Photocatalysis: Fundamentals, Materials and Potential*, 1st ed., MDPI, Basel, Switzerland, 2016.
- [4] J. Schneider, D. Bahnemann, J. Ye, G.L. Puma, D.D. Dionysiou (Eds.), *Photocatalysis: Fundamentals and Perspectives*, 1st ed., The Royal Society of Chemistry, Cambridge, UK, 2016.
- [5] J.C. Colmenares, Y.-J. Xu (Eds.), *Heterogeneous Photocatalysis: from Fundamentals to Green Applications*, 1st ed., Springer-Verlag, Berlin Heidelberg, 2016.
- [6] C. McCullagh, N. Skillen, M. Adams, P.K.J. Robertson, *J. Chem. Technol. Biotechnol.* 86 (2011) 1002–1017.
- [7] C. Minero, V. Maurino, D. Vione, *Photocatalytic mechanisms and reaction pathways drawn from kinetic and probe molecules*, in: P. Pichat (Ed.), *Photocatalysis and Water Purification*, Wiley-VCH Verlag GmbH & Co., KGaA, Weinheim, 2013, pp. 53–72.
- [8] P. Calza, C. Minero, E. Pelizzetti, *Environ. Sci. Technol.* 31 (1997) 2198–2203.
- [9] J.-M. Herrmann, *Catal. Today* 53 (1999) 115–129.
- [10] M.A. Henderson, *Surf. Sci. Rep.* 66 (2011) 185–297.
- [11] C. Minero, *Catal. Today* 54 (1999) 205–216.
- [12] J. Cunningham, G. Al-Sayyed, S. Srijaranai, G.R. Helz, *Adsorption of model pollutants onto  $\text{TiO}_2$  particles in relation to photoremediation of contaminated water*, in: G.R. Helz, R.G. Zepp, D.G. Crosby (Eds.), *Aquatic and Surface Photochemistry*, Taylor & Francis, Boca Raton, FL, USA, 1994, pp. 317–348.
- [13] Y. Xu, C.H. Langford, *J. Photochem. Photobiol. A-Chem.* 133 (2000) 67–71.

- [14] A.V. Emeline, V. Ryabchuk, N. Serpone, J. Photochem. Photobiol. A-Chem. 133 (2000) 89–97.
- [15] C. Minero, D. Vione, Appl. Catal. B: Environ. 67 (2006) 257–269.
- [16] A.V. Emeline, V.K. Ryabchuk, N. Serpone, J. Phys. Chem. B 109 (2005) 18515–18521.
- [17] M. Minella, F. Bertaina, C. Minero, Catal. Today 315 (2018) 9–18.
- [18] D. Monllor-Satoca, R. Gómez, M. González-Hidalgo, P. Salvador, Catal. Today 129 (2007) 247–255.
- [19] V. Maurino, A. Bedini, M. Minella, F. Rubertelli, E. Pelizzetti, C. Minero, J. Adv. Oxid. Technol. 11 (2008) 184–192.
- [20] S. Valencia, F. Cataño, L. Rios, G. Restrepo, J. Marín, Appl. Catal. B: Environ. 104 (2011) 300–304.
- [21] C. Minero, A. Bedini, V. Maurino, Appl. Catal. B: Environ. 128 (2012) 135–143.
- [22] T. Egerton, Molecules 19 (2014) 18192.
- [23] F. Pellegrino, L. Pellutiè, F. Sordello, C. Minero, E. Ortel, V.-D. Hodoroaba, V. Maurino, Appl. Catal. B: Environ. 216 (2017) 80–87.
- [24] F. Ramiro-Manzano, P. Atienzar, I. Rodriguez, F. Meseguer, H. Garcia, A. Corma, Chem. Commun. (2007) 242–244.
- [25] J.I.L. Chen, G. von Freymann, V. Kitaev, G.A. Ozin, J. Am. Chem. Soc. 129 (2007) 1196–1202.
- [26] F. Sordello, C. Duca, V. Maurino, C. Minero, Chem. Commun. 47 (2011) 6147–6149.
- [27] G. Camera-Roda, V. Augugliaro, A.G. Cardillo, V. Loddò, L. Palmisano, F. Parrino, F. Santarelli, Catal. Today 259 (2016) 87–96.
- [28] G. Camera-Roda, V. Loddò, L. Palmisano, F. Parrino, Catal. Today 281 (2017) 221–230.
- [29] A.K. Alexander, J. Phys. D 40 (2007) 2210.
- [30] G. Palmisano, V. Loddò, V. Augugliaro, M. Bellardita, G. Camera Roda, F. Parrino, Chem. Eng. J. 262 (2015) 490–498.
- [31] R.J. Brandi, M.A. Citroni, O.M. Alfano, A.E. Cassano, Chem. Eng. Sci. 58 (2003) 979–985.
- [32] K. Mehrotra, G.S. Yablonsky, A.K. Ray, Chemosphere 60 (2005) 1427–1436.
- [33] M. Minella, M. Demontis, M. Sarro, F. Sordello, P. Calza, C. Minero, J. Mater. Sci. 50 (2015) 2399–2409.
- [34] M.I. Cabrera, O.M. Alfano, A.E. Cassano, J. Phys. Chem. 100 (1996) 20043–20050.
- [35] P.S. Mudgett, L.W. Richards, Appl. Opt. 10 (1971) 1485–1502.
- [36] M.L. Satuf, R.J. Brandi, A.E. Cassano, O.M. Alfano, Ind. Eng. Chem. Res. 44 (2005) 6643–6649.
- [37] J.F. Montoya, J.A. Velásquez, P. Salvador, Appl. Catal. B: Environ. 88 (2009) 50–58.
- [38] W.H. Koppenol, J.D. Rush, J. Phys. Chem. 91 (1987) 4429–4430.
- [39] T.L. Villarreal, R. Gómez, M. González, P. Salvador, J. Phys. Chem. B 108 (2004) 20278–20290.
- [40] I. Mora-Seró, T.L. Villarreal, J. Bisquert, Á. Pitarch, R. Gómez, P. Salvador, J. Phys. Chem. B 109 (2005) 3371–3380.
- [41] N. Hykaway, W.M. Sears, H. Morisaki, S.R. Morrison, J. Phys. Chem. 90 (1986) 6663–6667.
- [42] S.R. Morrison, Electrochemistry at Semiconductor and Oxidized Metal Electrodes, Plenum Press, 1980.
- [43] T. Ohno, K. Sarukawa, K. Tokieda, M. Matsumura, J. Catal. 203 (2001) 82–86.
- [44] R.I. Bickley, T. Gonzalez-Carreno, J.S. Lees, L. Palmisano, R.J.D. Tilley, J. Solid State Chem. 92 (1991) 178–190.